Cepharanthine inhibits lysosomes and induces apoptosis in triple-negative breast cancer cells

JUAN LI[1,2], SIQIN ZHOU[1,2], YU WANG[1,2], GUANGHAN OU[1,2], DANLI YANG[1,2] and LIWEN SHEN[1,2]

[1]Key Laboratory of Basic Pharmacology of Ministry of Education, Zunyi Medical University, Zunyi, Guizhou 563000, P.R. China; [2]Joint International Research Laboratory of Ethnomedicine of Ministry of Education, Zunyi Medical University, Zunyi, Guizhou 563000, P.R. China

Received June 3, 2025; Accepted January 12, 2026

DOI: 10.3892/mmr.2026.13899

Abstract. Triple-negative breast cancer (TNBC) is an aggressive malignancy with limited treatment options and a poor prognosis. The present study investigated the anti-TNBC effects and underlying mechanisms of cepharanthine (CEP), an isoquinoline alkaloid derived from *Stephania cephalantha*. The findings showed that CEP inhibited colony formation and induced apoptosis in TNBC cells. Mechanistic investigations revealed that CEP upregulated the pro-apoptotic protein phorbol-12-myristate-13-acetate-induced protein 1 (NOXA), downregulated the anti-apoptotic protein Bcl-2 and reduced the mitochondrial membrane potential ($\Delta\Psi m$). Using quantitative proteomics and limited proteolysis-coupled mass spectrometry, the present study demonstrated that CEP bound directly to the lysosomal enzymes cathepsin B and cathepsin D, thereby impairing their maturation and suppressing lysosomal degradation. This inhibition triggered the nuclear accumulation of transcription factor EB (TFEB), a factor that regulates the expression of Bcl-2 family members. These findings indicated that CEP induced apoptosis by inhibiting lysosomal function and activating TFEB, leading to the upregulation of NOXA and downregulation of Bcl-2. In conclusion, the present study demonstrated the pro-apoptotic effect of CEP in TNBC cells and identified lysosomal enzymes as the direct target for its mechanism of action. These findings provided a foundation for further investigation of the pharmacological mechanisms of CEP.

Correspondence to: Professor Danli Yang or Professor Liwen Shen, Key Laboratory of Basic Pharmacology of Ministry of Education, Zunyi Medical University, 6 Xuefu West Road, Xinpu New District, Zunyi, Guizhou 563000, P.R. China
E-mail: yangdanli@zmu.edu.cn
E-mail: shenliwen@zmu.edu.cn

Key words: cepharanthine, triple-negative breast cancer, lysosome, cathepsin, phorbol-12-myristate-13-acetate-induced protein 1, apoptosis

Introduction

Triple-negative breast cancer (TNBC) is defined as a breast cancer subtype that lacks expression of estrogen receptor, progesterone receptor and human epidermal growth factor receptor 2 (1). Compared with other subtypes, TNBC typically exhibits higher Ki-67 antigen expression, a greater mitotic index, more frequent breast cancer susceptibility gene 1 mutations and a more aggressive clinical course (2). In the United States, the mean annual incidence is ~13.7 per 100,000 women. Higher frequencies are observed among African American and Hispanic women, as well as in women with younger age, higher premenopausal body mass index, earlier age at menarche, higher parity and a history of oral contraceptive use (2-4). Notably, TNBC is associated with the lowest 5-year locoregional recurrence-free survival (79.6%) and local recurrence-free survival (84.6%) among all breast cancer subtypes (5). The lack of expression of targetable receptors in TNBC markedly restricts therapeutic options, with current management primarily involving surgical resection, radiotherapy and chemotherapeutic agents such as paclitaxel and doxorubicin (6). This constraint in treatment options underscores the need to explore new targets and develop innovative therapies for TNBC.

Cepharanthine (CEP), a bisbenzylisoquinoline alkaloid derived from *Stephania cephalantha*, has a wide range of pharmacological activities, including anti-severe acute respiratory syndrome coronavirus 2, immunomodulatory, anti-atherosclerotic and antitumor properties (7). CEP also has notable antiproliferative and pro-apoptotic activities in cancer cell lines, such as those derived from hepatocellular carcinoma and colorectal cancer (8). These effects may be mediated by the influence of CEP on important signaling pathways, such as the PI3K/Akt, MAPK and NF-κB pathways, and its modulation of Bcl-2 family protein expression (8). Despite these well-documented antitumor effects, the direct molecular targets of CEP remain poorly defined. The aims of the present study were to evaluate the efficacy of CEP against TNBC *in vitro* and elucidate its mechanisms of action, with a specific focus on identifying the direct molecular targets.

Materials and methods

Cell culture. All cell lines were maintained at 37˚C in 5% CO_2 atmosphere and tested routinely for mycoplasma contamination.

The TNBC cell lines MDA-MB-231 (cat. no. CL-0150; Procell Life Science & Technology Co., Ltd.) and Hs578T (cat. no. CL-0114; Procell Life Science & Technology Co., Ltd.) were cultured in high-glucose DMEM medium (cat. no. C11965500BT; Gibco; Thermo Fisher Scientific, Inc.), supplemented with 10% fetal bovine serum (cat. no. 164210; Procell Life Science & Technology Co., Ltd.) and 1% penicillin/streptomycin (cat. no. 15140122; Gibco; Thermo Fisher Scientific, Inc.). The Hs578T cultures were also supplemented with 10 μg/ml insulin (cat. no. P3376; Beyotime Institute of Biotechnology). The human normal breast epithelial cell line MCF10A (cat. no. CL-0525; Procell Life Science & Technology Co., Ltd.) was cultured in commercially pre-configured DMEM/F12 medium (cat. no. CM-0525; Procell Life Science & Technology Co., Ltd.) which was supplemented with 5% donor equine serum, 20 ng/ml epidermal growth factor, 0.5 μg/ml hydrocortisone, 10 μg/ml insulin, 1% non-essential amino acid solution and 1% penicillin/streptomycin. Only low-passage cells (<15 passages) were used in all the experiments.

Cytotoxicity assay. The cytotoxicity of CEP (purity, 99.06%; cat. no. A0653; Chengdu Must Bio-Technology Co., Ltd.) was evaluated via the Cell Counting Kit-8 (CCK-8) assay. Briefly, MDA-MB-231, Hs578T and MCF10A cells were seeded in 96-well plates at a density of 4,000 cells per well and treated with various concentrations (1, 2, 4, 6, 8, 10, 15, 20, 25 and 30 μM) of CEP for 24, 48 or 72 h at 37˚C. A 10 μl aliquot of CCK-8 reagent (cat. no. C0005; TargetMol Chemicals Inc.) was then added to each well and the plates were incubated for 1 h at 37˚C. The absorbance at 450 nm was measured using a Multiskan FC microplate reader (Thermo Fisher Scientific, Inc.). Dose-response curves and IC_{50} values were generated using GraphPad Prism (version 9.0.0; Dotmatics).

Clonogenicity assay. MDA-MB-231 and Hs578T cells were seeded in 6-well plates at 400 cells per well and incubated for 48 h at 37˚C. The medium was then replaced with fresh medium containing CEP (2, 4, 8, 15 and 30 μM for MDA-MB-231; 1, 2, 4, 8 and 15 μM for Hs578T), followed by 12 days of incubation at 37˚C, with the medium being refreshed every 3 days. At the end of treatment, colonies were fixed with 4% paraformaldehyde (cat. no. P0098; Beyotime Institute of Biotechnology) for 5 min, stained with 1% crystal violet for 30 min room temperature (RT), then air dried at RT. Images of the colonies were recorded using a ChemiDoc MP imaging system (Bio-Rad Laboratories, Inc.) and the number of colonies was counted manually. For counting purposes, a colony was defined as a cell aggregate having an area >0.05 mm^2.

TUNEL assay. MDA-MB-231 and Hs578T cells were seeded in 24-well plates at a density of $1x10^4$ cells per well and treated with 10 μM CEP for 24 h at 37˚C. Following two PBS washes, cells were fixed with 4% paraformaldehyde (cat. no. P0098; Beyotime Institute of Biotechnology) for 15 min at RT, permeabilized with 0.1% Triton X-100 (cat. no. P0097; Beyotime Institute of Biotechnology) for 10 min at RT and subsequently analyzed using a One-step TUNEL Apoptosis Assay Kit (cat. no. C1088; Beyotime Institute of Biotechnology) according to the manufacturer's instructions. The cell nuclei were stained with 50 μl of DAPI medium (10 μg/ml) (cat. no. P0131; Beyotime Institute of Biotechnology) for 10 min at RT, mounted with 50 μl of anti-fade mounting medium (cat. no. P0126; Beyotime Biotechnology), and then imaged using a fluorescence microscope (IX73; Olympus Corporation), with DAPI excitation/emission set at 358/461 nm and FITC excitation/emission at 495/519 nm. Images from three randomly selected fields of view per well were captured for the subsequent analysis of the percentage of TUNEL-positive cells.

Flow cytometry analysis. MDA-MB-231 and Hs578T cells were seeded in 6-well plates at $1x10^6$ cells per well and exposed to CEP (5, 10 and 20 μM for MDA-MB-231; 2, 4 and 8 μM for Hs578T) for 48 h at 37˚C. Following treatment, the cells and supernatant were collected, centrifuged at 1,000 x g for 5 min at RT and the supernatant was subsequently discarded. The cell pellet was washed with PBS and resuspended in 195 μl of annexin V-FITC binding buffer (cat. no. C1062L; Beyotime Institute of Biotechnology). A total of 5 μl annexin V-FITC was subsequently added to cells with gentle mixing, followed by 10 μl propidium iodide, also administered with gentle mixing. The samples were incubated at RT in the dark for 15 min and apoptosis was subsequently assessed using a flow cytometer (EPICS® XL™; Beckman Coulter, Inc.). The results were analyzed using FlowJo software (version 10.8.1; FlowJo LLC; BD Biosciences).

Mitochondrial membrane potential ($\Delta\Psi m$) assay. MDA-MB-231 and Hs578T cells were seeded in 35 mm glass-bottom dishes at a density of $2x10^5$ cells per dish and treated with CEP (10 μM for MDA-MB-231, and 4 μM for Hs578T) for 24 h at 37˚C. Following two PBS washes, cells were incubated with 5 μg/ml 5,5',6,6'-tetrachloro-1,1',3,3'-tetraethylbenzimidazolylcarbocyanine iodide (JC-1) (cat. no. T15609; TargetMol Chemicals Inc.) for 20 min at 37˚C. The fluorescence of the cells was visualized using a fluorescence microscope, with JC-1 monomer excitation/emission set at 510/527 nm and JC-1 aggregate excitation/emission set at 585/590 nm. The shift from red (aggregates) to green (monomers) fluorescence indicated mitochondrial depolarization.

Western blot analysis. MDA-MB-231 and Hs578T cells were cultured in 10-cm dishes and treated with different concentrations of CEP (5, 10 and 20 μM for MDA-MB-231; 2, 4 and 8 μM for Hs578T) for 24 h at 37˚C. The cells were lysed in RIPA buffer (cat. no. P0013B; Beyotime Institute of Biotechnology) at 0˚C for 20 min before centrifugation at 16,000 x g for 10 min at 4˚C. Supernatant protein concentrations were subsequently determined via BCA assay. Equal amounts of protein (20 μg per lane) were denatured for 7 min at 100˚C and then separated by 12% SDS-PAGE gels at 80 V for 40 min and 120 V for 60 min. Proteins were subsequently transferred to 0.45-μm PVDF membranes using a Trans-Blot Turbo semi-dry system (1.3 A; 25 V; 10-20 min; Bio-Rad Laboratories, Inc.). The membranes were subsequently treated with QuickBlock™ western blocking buffer (cat. no. P0220; Beyotime Biotechnology) for 30 min at RT and incubated overnight at 4˚C with the following primary antibodies (all in a 1:1,000 dilution): Acid ceramidase (ASAH1; cat. no. 11274-1-AP; Proteintech Group, Inc.), sphingomyelin phosphodiesterase (SMPD1; cat. no. 14609-1-AP; Proteintech Group, Inc.), cathepsin B (CTSB; cat. no. 112216-1-AP; Proteintech

Group, Inc.), cathepsin D (CTSD; cat. no. 21327-1-AP; Proteintech Group, Inc.), phorbol-12-myristate-13-acetate-induced protein 1 (NOXA; cat. no. 14766; Cell Signaling Technology, Inc.), Bax (cat. no. 2772T; Cell Signaling Technology, Inc.), Bcl-2 (cat. no. 15071T; Cell Signaling Technology, Inc.) and cleaved caspase-3 (cat. no. 9661T; Cell Signaling Technology, Inc.). After washing in TBST containing 0.1% Tween-20 (v/v), the membranes were incubated with HRP-conjugated secondary antibodies (1:5,000 dilution; cat. no. SA00001-2; Proteintech Group, Inc.) for 1 h at RT, followed by detection using the Tanon™ ECL chemiluminescent substrate (cat. no. 180-501; Shanghai Tanon Life Science Co., Ltd.). The membranes were then placed in stripping buffer (cat. no. SW3022; Beijing Solarbio Science & Technology Co., Ltd.) for 3 min and re-probed with anti-β-actin antibody (cat. no. 66009-1-Ig; Proteintech Group, Inc.) as the loading control. Semi-quantitative analysis of the band/intensity was performed using ImageJ software (version 1.53t; National Institutes of Health).

Proteomics analysis. MDA-MB-231 cells at 80% confluence in 10 cm dishes were treated with 10 μM CEP or 0.1% DMSO for 24 h at 37˚C and then harvested by scraping on ice. Cells were subject to lysis in urea buffer (8 M urea; 1% PMSF) using pulsed ultrasonication (200 W; 3 sec on, 10 sec off; 40 cycles) and centrifuged at 12,000 x g at 4˚C for 10 min. The protein content of the supernatants was quantified using the BCA assay. Following precipitation with 20% trichloroacetic acid at 4˚C for 2 h, the protein isolates were washed three times with ice-cold acetone and then digested overnight with trypsin (cat. no. V5280; Promega Corporation) at a 1:50 enzyme-to-protein ratio at 37˚C, followed by resuspension in 200 mM tetraethylammonium bromide solution. The isolated peptides were reduced with 5 mM dithiothreitol at 56˚C for 30 min and then alkylated with 11 mM iodoacetamide at RT for 15 min. The samples were then dissolved in mobile phase A in 0.1% formic acid and 2% acetonitrile in water, before samples were separated by nano-ultra-high performance liquid chromatography (UHPLC) (Bruker Corporation) using a linear gradient of solvent B (0.1% formic acid in acetonitrile/water). The gradient was as follows: 6-24% solvent B (0-14 min), 24-35% solvent B (14-16 min), 35-80% solvent B (16-18 min) and 80% solvent B (18-20 min) at 500 nl/min.

The separated peptides were analyzed using a timsTOF Pro 2 mass spectrometer (Bruker Corporation) in data-independent acquisition (DIA) parallel accumulation serial fragmentation (PASEF) mode. Full MS scans (m/z, 300-1500) were acquired, followed by 20 PASEF MS/MS scans per cycle for a total of 32 cycles (isolation window, 7 m/z; scan range, m/z 400-850). The data were processed using the DIA-NN search engine (version 1.8) (9) and the *Homo sapiens* UniProt database (taxon identifier, 9606; release, 2023_12; downloaded from https://www.uniprot.org/proteomes/UP000005640 in December 2023) concatenated with a reverse decoy database. Trypsin was set as the cleavage enzyme with one missed cleavage allowed. Fixed modifications included N-terminal methionine excision and cysteine carbamidomethylation. The false discovery rate (FDR) was controlled at <1%, with a quantitative analysis subsequently conducted using the robust label-free quantification algorithm of DIA-NN. Differentially expressed proteins (DEPs) were identified by a fold change (FC) <0.667 or >1.5 and P<0.05. Functional annotation of the DEPs was performed using Gene Ontology (GO) enrichment and the Kyoto Encyclopedia of Genes and Genomes (KEGG) pathway analyses via the DAVID Bioinformatics Resources (https://david.ncifcrf.gov/) and the KEGG database (https://www.genome.jp/kegg/), respectively.

Immunofluorescence analysis. MDA-MB-231 and Hs578T cells were seeded in 35-mm glass-bottom dishes at a density of $2x10^5$ cells per dish and treated with CEP (10 μM for MDA-MB-231, and 4 μM for Hs578T) for 24 h at 37˚C. The cells were fixed with 4% paraformaldehyde (cat. no. P0098; Beyotime Institute of Biotechnology) for 15 min at RT, permeabilized with 0.1% Triton X-100 (cat. no. P0097; Beyotime Institute of Biotechnology) for 10 min at RT, and after blocking with serum-free QuickBlock™ blocking buffer (cat. no. P0260; Beyotime Biotechnology) for 30 min at RT, incubated with transcription factor EB (TFEB) primary antibody (1:200; cat. no. 13372-1-AP; Proteintech Group, Inc.) overnight at 4˚C. The cells were then stained with CoraLite594-conjugated secondary antibody (1:200 dilution; cat. no. SA00013-4; Proteintech Group, Inc.) for 1 h at RT and DAPI (10 μg/ml) for 10 min at RT. Images were recorded via confocal microscopy (STELLARIS 5; Leica Microsystems, Inc.) with the following settings: CoraLite594 excitation/emission, 588/604 nm; and DAPI excitation/emission, 358/461 nm. For each experimental condition, the nuclear-to-cytoplasmic ratio of TFEB and TFE3 was determined in 5 randomly selected cells using ImageJ software. The DAPI channel defined the nuclear region, and a 2-μm expansion from this boundary defined the cytoplasmic region for intensity measurement.

Lysosomal membrane integrity assay. MDA-MB-231 and Hs578T cells were seeded in 35-mm glass-bottom dishes at a density of $2x10^5$ cells per dish. The lysosomes were pre-loaded with 100 μg/ml Alexa Fluor™ 488-dextran (cat. no. D22910; Thermo Fisher Scientific, Inc.) for 6 h at 37˚C, followed by a 2-h incubation in fresh DMEM medium at 37˚C. After treatment for 24 h with CEP (10 μM for MDA-MB-231, and 4 μM for Hs578T), the retention of dextran within the lysosomes was assessed by confocal microscopy (STELLARIS 5; Leica Microsystems, Inc.; Alexa Fluor 488 excitation/emission, 495/519 nm). This provided a marker of membrane integrity.

Lysosomal pH assay. MDA-MB-231 and Hs578T cells were seeded in 35-mm glass-bottom dishes at a density of $2x10^5$ cells per dish and exposed to CEP (10 μM for MDA-MB-231, and 4 μM for Hs578T) for 24 h at 37˚C. Lysosomal pH was measured by incubating the cells with 2 μM LysoSensor™ Green DND-189 (cat. no. 40767ES50; Shanghai Yeasen Biotechnology Co., Ltd.) for 5 min at 37˚C, followed by washing with PBS and immediate image capture of fluorescence via confocal microscopy (STELLARIS 5; Leica Microsystems, Inc.); LysoSensor Green DND-189 excitation/emission, 443/505 nm).

Limited proteolysis-coupled mass spectrometry (LiP-MS) assay. This assay was conducted using MDA-MB-231 cells. MDA-MB-231 cells were treated with 10 μM CEP or 0.1% DMSO for 1 h at 37˚C, harvested by ice-cold scraping, lysed in sodium deoxycholate buffer (5% sodium deoxycholate; 1 mM KH_2PO_4; 3 mM Na_2HPO_4; 155 mM NaCl; pH 7.5)

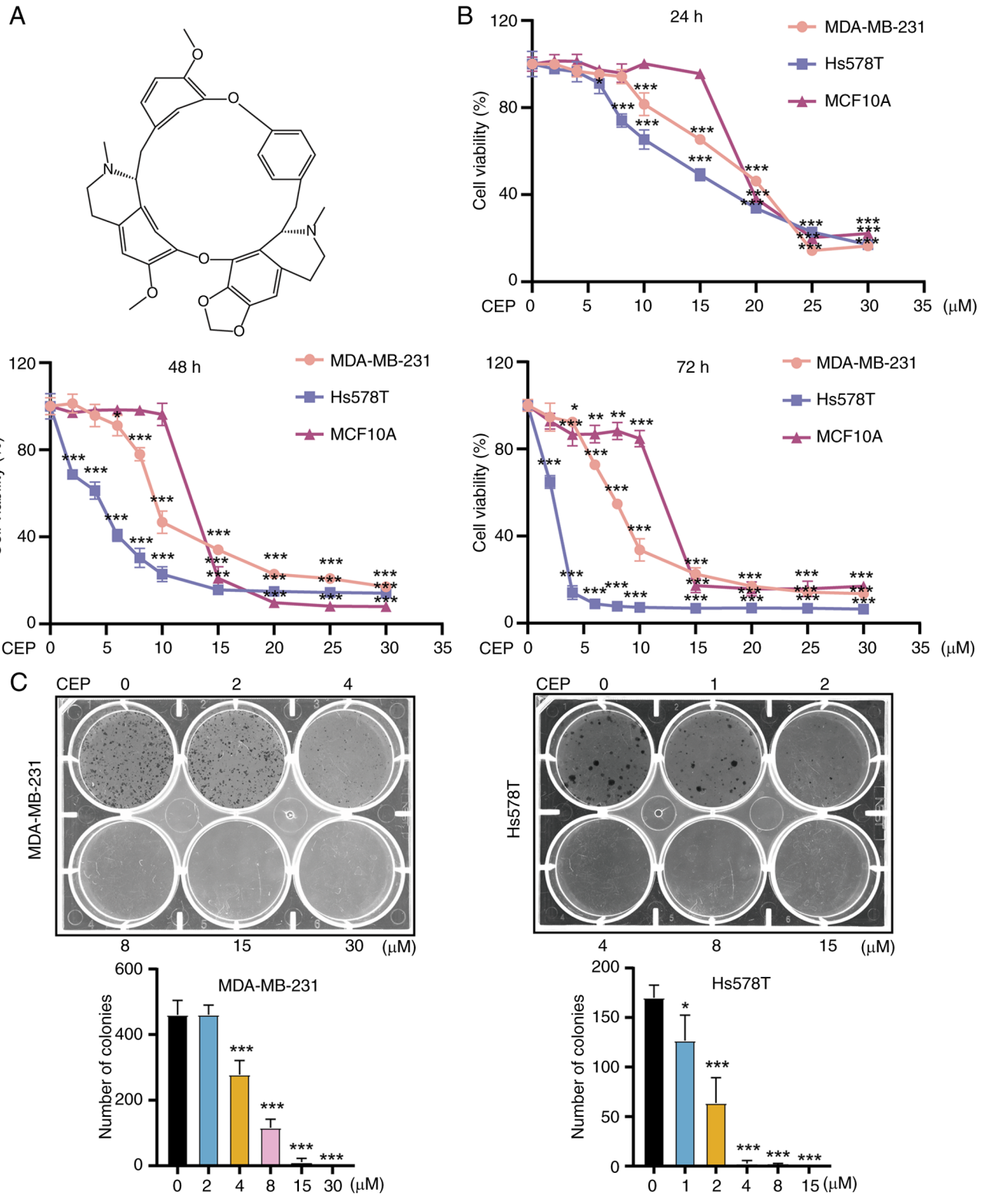

Figure 1. CEP exerts cytotoxicity in TNBC cells. (A) Chemical structure of CEP. (B) CEP inhibited TNBC cell viability. The effect of CEP treatment on TNBC cell viability after 24, 48 and 72 h. (C) CEP inhibited clonogenicity of MDA-MB-231 and Hs578T cells. n=3; *P<0.05, **P<0.01 and ***P<0.001 vs. control. CEP, cepharanthine; TNBC, triple-negative breast cancer.

and centrifuged at 16,000 x g for 10 min at 4˚C. The cleared lysates were quantified via BCA assay and processed as followed in parallel: i) The LiP group was subject to proteinase K (cat. no. P4850; Sigma-Aldrich; Merck KGaA) digestion (1:100) at 25˚C for 1 h, followed by heat inactivation at 100˚C for 5 min; and ii) the trypsin (TrP) only control group. All samples (both LiP and TrP groups) were denatured with 1% sodium deoxycholate at 95˚C for 10 min, reduced with 10 mM tris(2-carboxyethyl)phosphine for 10 min at RT, and following pH adjustment to a pH of 9, digested sequentially with C-terminal lysin (1:100; cat. no. VA1170; Promega Corporation) at 37˚C for 4 h and trypsin (1:100) at 37˚C

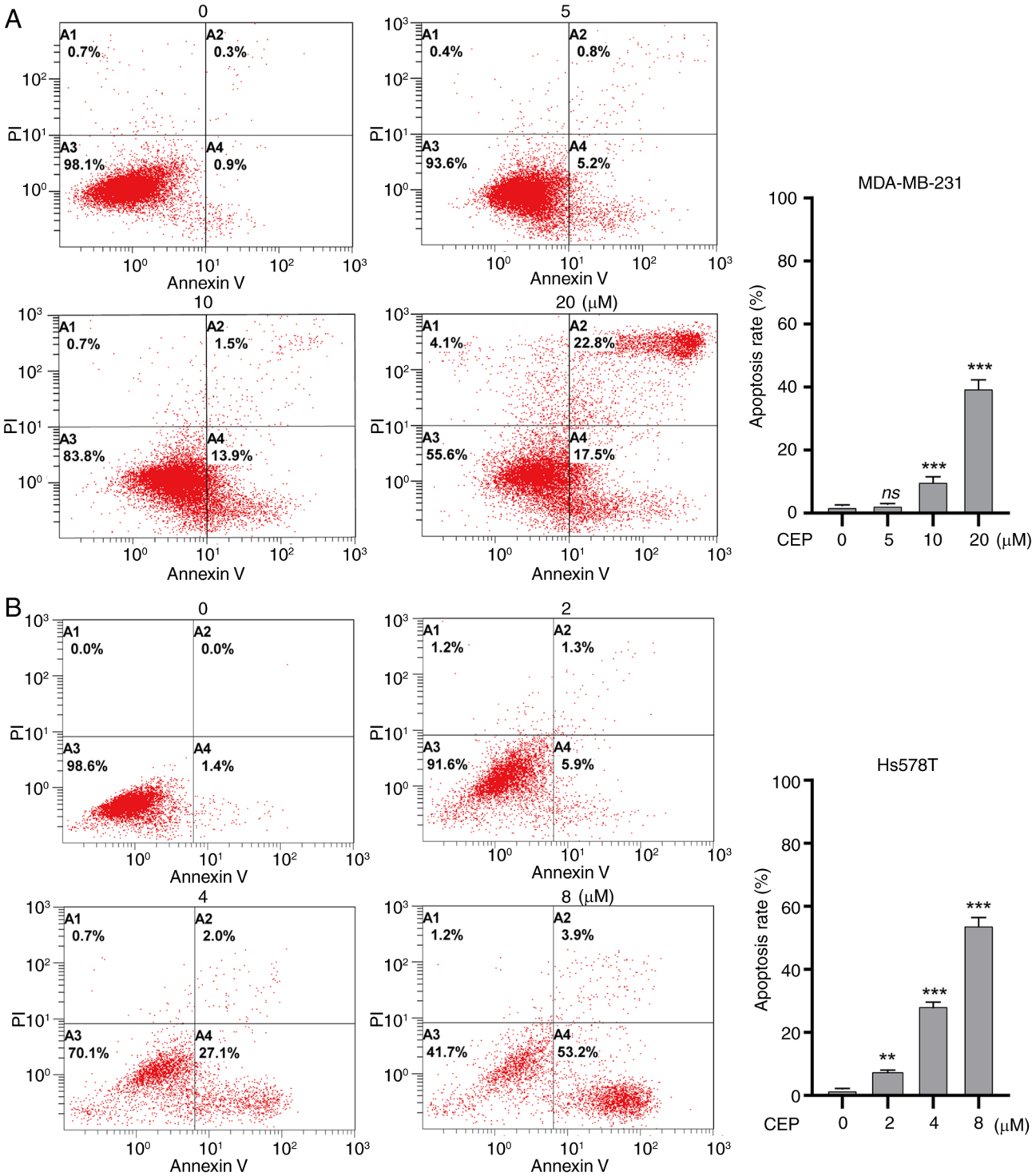

Figure 2. CEP induces apoptosis in triple-negative breast cancer cells. Flow cytometric quantification of apoptosis induced by CEP in (A) MDA-MB-231 and (B) Hs578T cells (n=3; 48 h). **P<0.01 and ***P<0.001 vs. control. CEP, cepharanthine; ns, not significant.

overnight. The isolated peptides were then acidified to pH≤3 with formic acid, centrifuged at 16,000 x g for 10 min at 4˚C, desalted using Monospin C18 columns (cat. no. 5010-21700; GL Sciences Inc.) and subsequently vacuum-dried.

For the MS analysis, the samples were dissolved in 0.1% formic acid and loaded onto a pulled-tip analytical column (cat. no. 00G-4053-B0; Phenomenex Inc.) connected to an Easy-nLC 1200 UHPLC system (Thermo Fisher Scientific, Inc.). The mobile phase consisted of solvent A (0.1% formic acid in water) and solvent B (0.1% formic acid in 80% acetonitrile). The peptides were separated using the following gradient: 0-1 min, 8% B; 1-8 min, 12% B; 8-63 min, 30% B; 63-75 min, 40% B; 75-76 min, 95% B; and 76-90 min, 95% B (flow rate, 300 nl/min). The eluted peptides were then electrosprayed into a Q Exactive HF-X (Thermo Fisher Scientific, Inc.), allowing for acquisition of full-scan MS spectra (m/z, 350-1,500) at a resolution of 120,000 (m/z, 200), with the top 40 precursor ions being selected

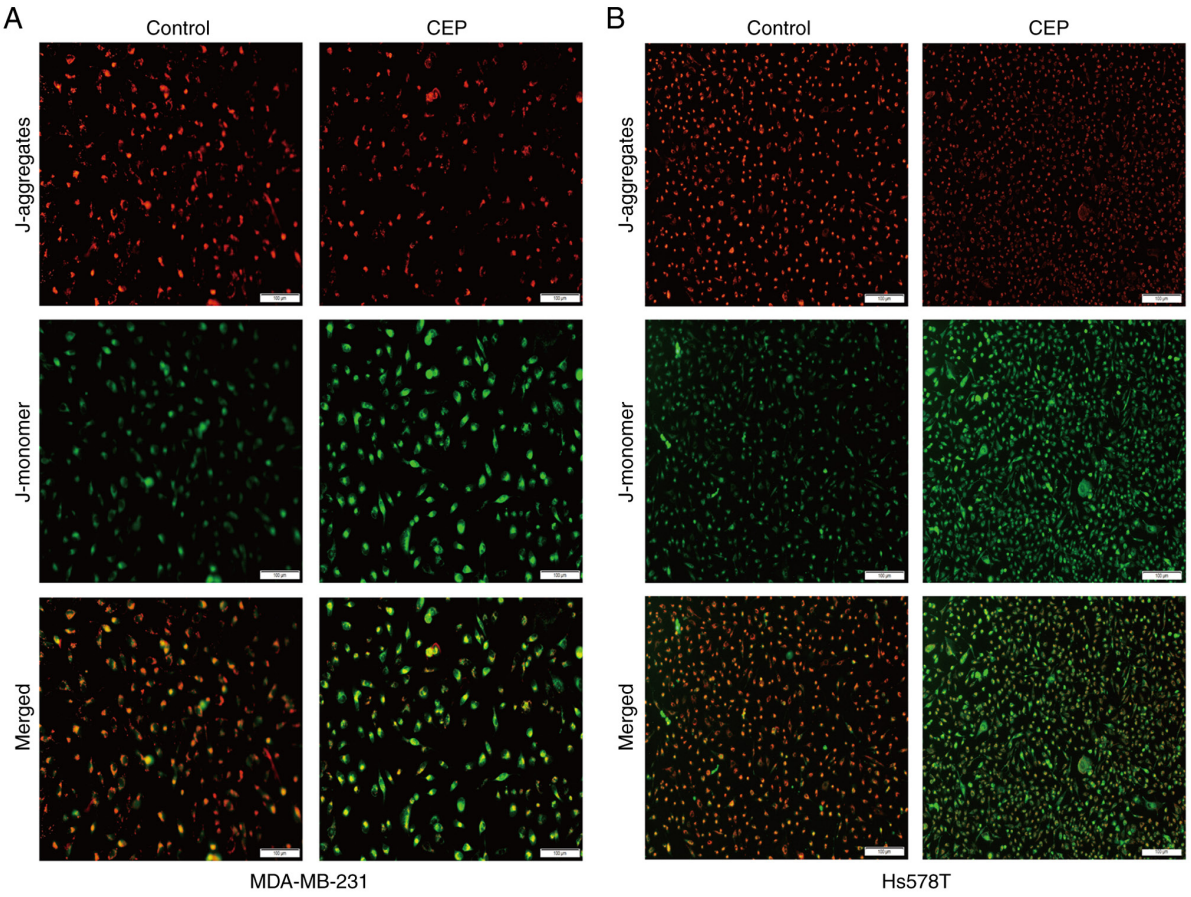

Figure 3. CEP induces ΔΨm loss in triple-negative breast cancer cells. (A) MDA-MB-231 (10 μM; n=3; 24 h) and (B) Hs578T cells (4 μM; n=3; 24 h). Scale bar, 100 μM. CEP, cepharanthine.

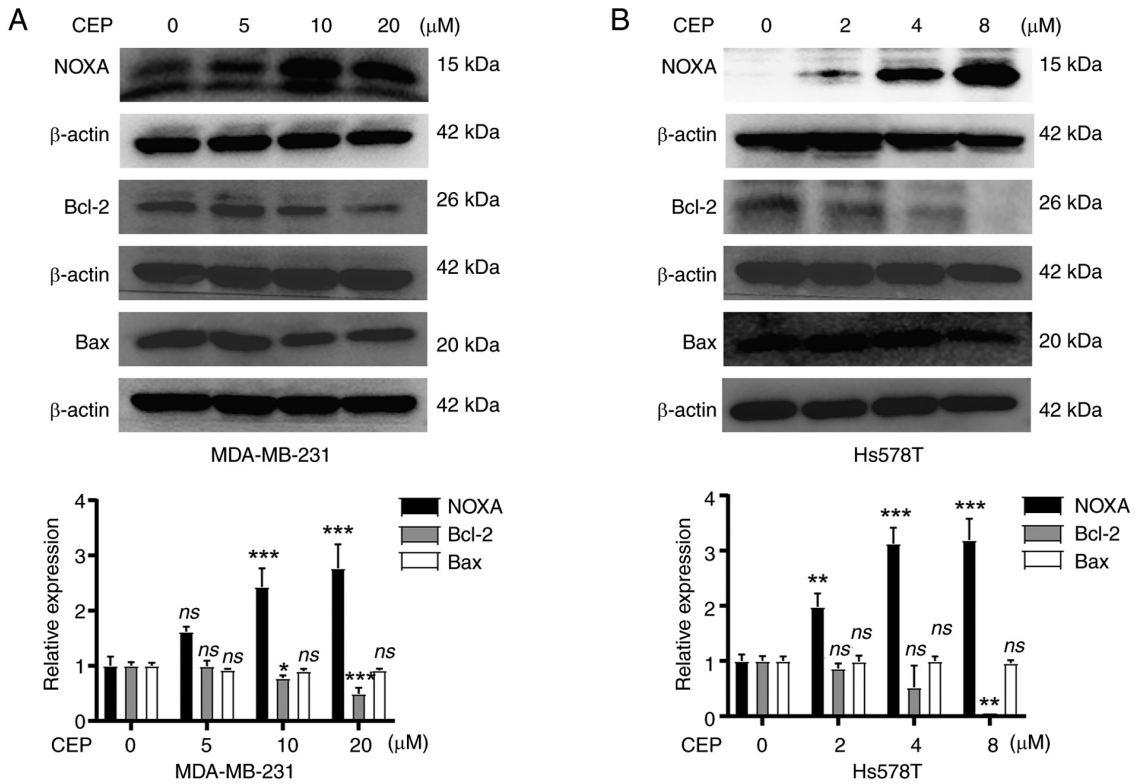

Figure 4. CEP upregulates NOXA and downregulates Bcl-2 expression in triple-negative breast cancer cells. CEP upregulated NOXA and downregulated Bcl-2 expression in (A) MDA-MB-231 cells (n=3; 24 h) and (B) Hs578T cells (n=3; 24 h). *P<0.05, **P<0.01 and ***P<0.001 vs. control. CEP, cepharanthine; NOXA, phorbol-12-myristate-13-acetate-induced protein 1; ns, not significant.

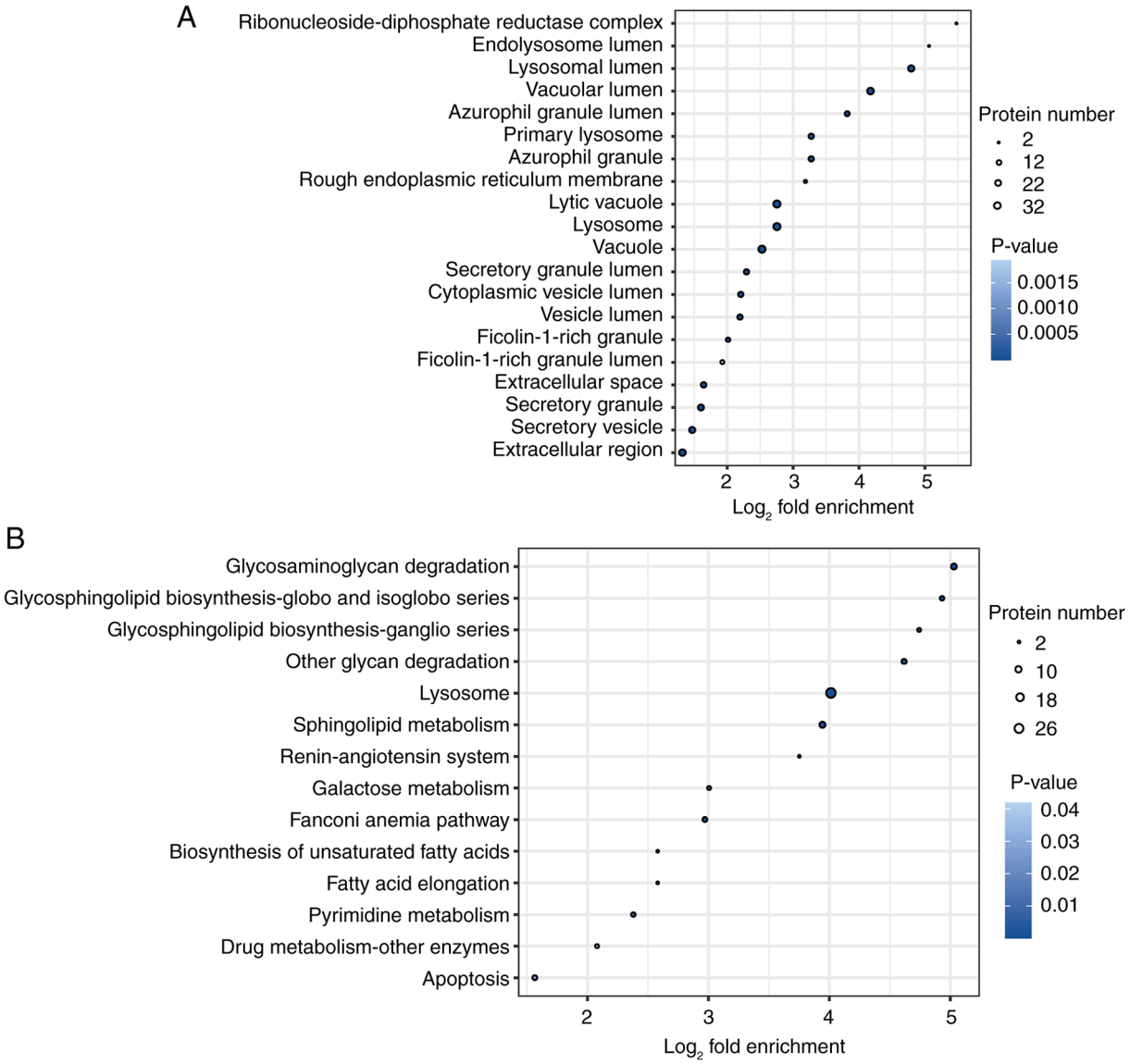

Figure 5. Proteomic profiling of MDA-MB-231 cells following CEP treatment. (A) The 20 most significantly downregulated Gene Ontology cellular components with CEP treatment. (B) Significantly downregulated Kyoto Encyclopedia of Genes and Genomes pathways with CEP treatment. CEP, cepharanthine.

for higher-energy C-trap dissociation (MS/MS resolution, 15,000; m/z, 200).

The data were processed using Proteome Discoverer (version 2.4; Thermo Fisher Scientific, Inc.) with the following parameters: Precursor mass tolerance of ±10 ppm, fragment mass tolerance of ±0.02 Da and fixed modification that included carbamidomethylation of cysteine (+57.0214 Da). Oxidation of methionine (+15.9949 Da) was set as the dynamic modification. The analysis allowed for up to two missed cleavages and maintained an FDR threshold of 1%. The abundance of individual peptides was normalized, imputed, corrected and analyzed for differential expression using a two-tailed Student's t-test (P<0.01 and FC >1.5 or <0.667).

Statistical analysis. The data are presented as mean±standard deviation from three biological replicates. Statistical analyses were performed using GraphPad Prism (version 9.0.0; Dotmatics). For comparisons between two groups, unpaired two-tailed Student's t-tests were used. For comparisons of ≥3 groups, one-way ANOVA was performed, followed by Dunnett's post hoc test for multiple comparisons. P<0.05 was considered to indicate a statistically significant difference.

Results

CEP induces apoptosis in TNBC cells. CEP (Fig. 1A) showed dose- and time-dependent cytotoxicity against both TNBC cell lines (Fig. 1B), with IC_{50} values after 48 h treatment of 9.37±0.55 μM for MDA-MB-231 and 6.07±0.31 μM for Hs578T. The IC_{50} for the normal human breast epithelial cell line MCF10A was 13.21±0.54 μM at 48 h. CEP treatment at higher doses resulted in the clonogenic formation of TNBC cells being suppressed significantly compared with untreated cells (Fig. 1C). Flow cytometric analysis also provided evidence that CEP treatment significantly induced apoptosis in TNBC cells (Fig. 2), and consistent with this finding, CEP treatment resulted in a significant increase in TUNEL-positive cells and caspase-3 activation (Fig. S1).

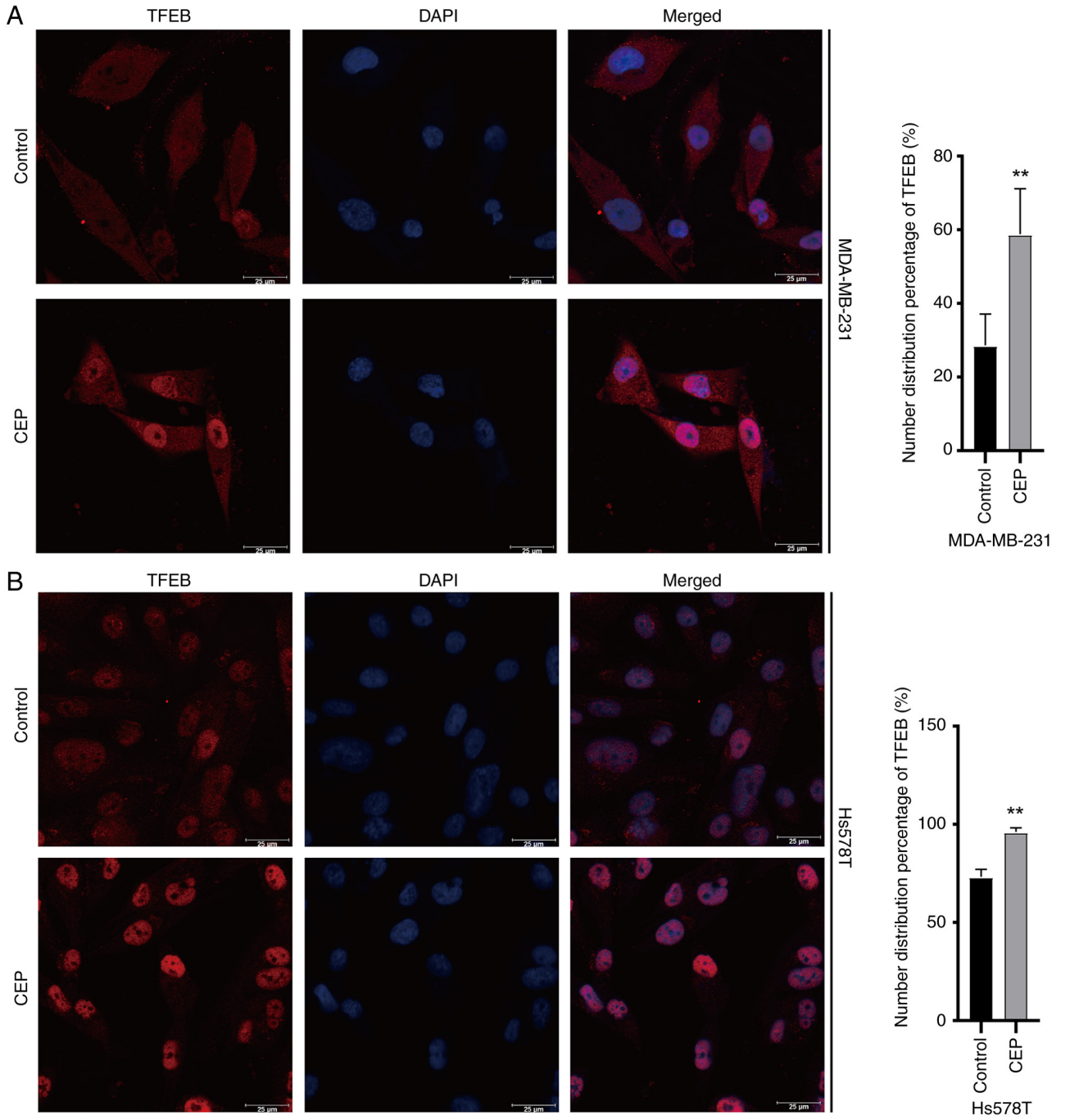

Figure 6. CEP treatment activates TFEB in triple-negative breast cancer cells. (A) CEP triggers TFEB nuclear translocation in MDA-MB-231 cells (10 μM; 24 h). (B) CEP triggers TFEB nuclear translocation in Hs578T cells (4 μM; 24 h). Scale bar, 25 μm; n=5. **P<0.01 vs. control. TFEB, transcription factor EB; CEP, cepharanthine.

Given that the collapse of the ΔΨm is an important event in the intrinsic apoptotic pathway (10), the present study subsequently assessed the effect of CEP on ΔΨm and observed that CEP triggered notable ΔΨm depolarization, as evidenced by a marked increase in JC-1 monomer fluorescence and a complementary decrease in aggregate fluorescence (Fig. 3). Given that the Bcl-2 protein family is a key regulator of mitochondrial apoptosis through regulation of ΔΨm (11), the present study examined the expression of relevant apoptosis-related proteins. Among the Bcl-2 family proteins examined, CEP treatment significantly upregulated the pro-apoptotic protein NOXA and downregulated the anti-apoptotic protein Bcl-2, whereas no significant change was observed in the expression of Bax (Fig. 4). Taken together, these results demonstrated that CEP induced apoptosis in TNBC cells, at least in part, by modulating the expression of NOXA and Bcl-2, leading to mitochondrial dysfunction.

CEP binds to and inhibits lysosomal enzymes in TNBC cells. The present study used quantitative proteomics to investigate the mechanism of action of CEP. In MDA-MB-231 cells, CEP treatment significantly altered the expression of 634 proteins, of which 521 were upregulated and 113 were downregulated

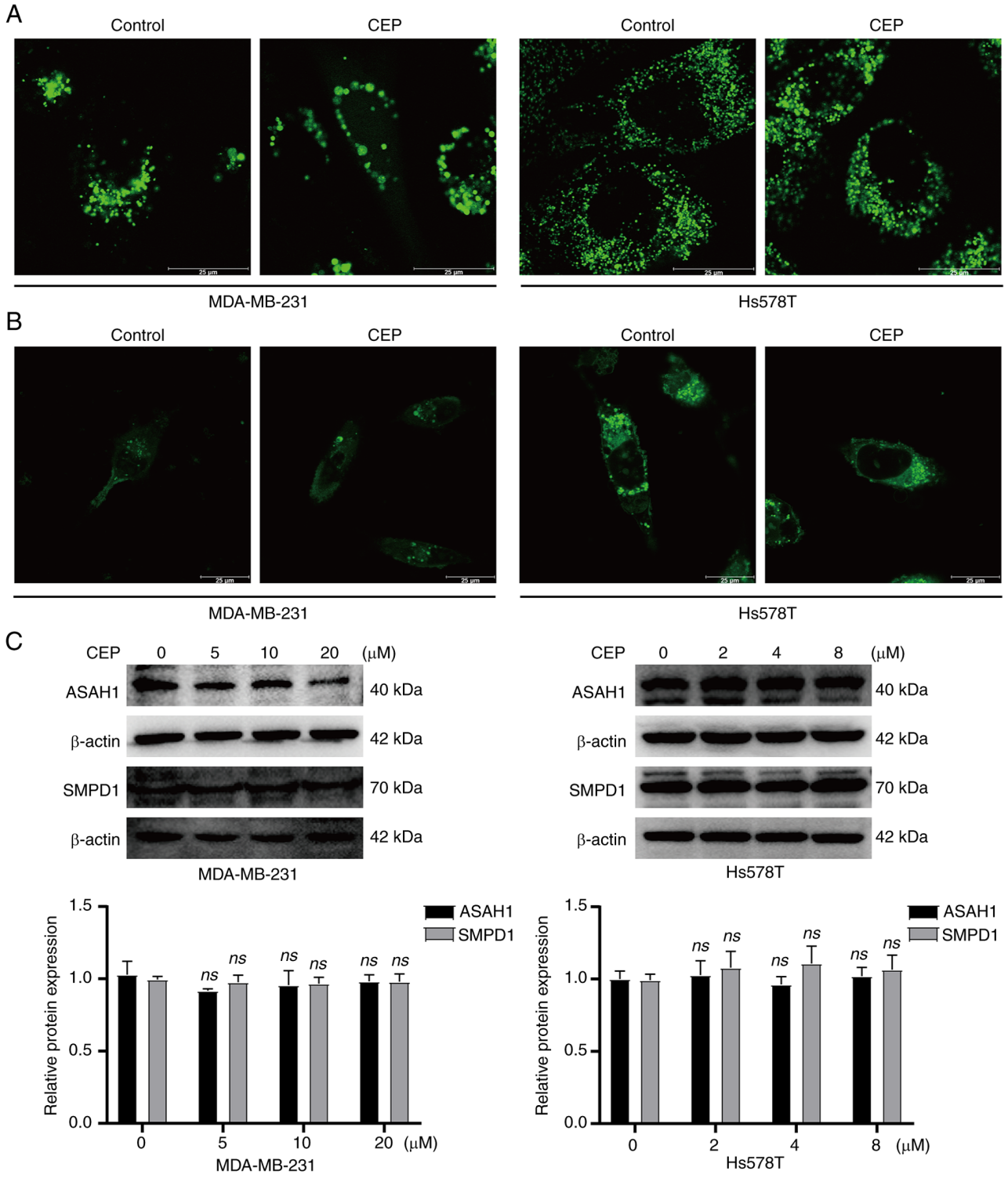

Figure 7. CEP does not induce LMP, increase lysosomal pH or destabilize lysosomal membrane-bound enzymes in triple-negative breast cancer cells. (A) CEP does not induce LMP, as evidenced by a dispersion of dextran, in MDA-MB-231 (10 μM; 24 h) and Hs578T cells (4 μM; 24 h). Scale bar, 25 μm. (B) CEP does not elevate lysosomal pH in the MDA-MB-231 (10 μM; 24 h) and Hs578T cell lines (4 μM; 24 h). Scale bar, 25 μm. (C) CEP does not induce lysosomal membrane-bound enzymes degradation in the MDA-MB-231 (10 μM; n=3; 24 h) and Hs578T cell lines (4 μM; n=3; 24 h). CEP, cepharanthine; ASAH1, acid ceramidase; SMPD1, sphingomyelin phosphodiesterase; ns, not significant.

(Table SI). GO and KEGG enrichment analyses indicated a notable enrichment of lysosomal pathways among the down-regulated proteins (Fig. 5), suggesting that CEP impaired lysosomal integrity or function. Consistent with this finding, confocal microscopy showed that CEP treatment triggered a significant increase in the nuclear accumulation of TFEB, the master regulator of lysosomal biogenesis, compared with the control group (Fig. 6). This result further supported the interpretation that CEP compromised lysosomal function and activated the lysosomal stress response.

Weakly basic compounds can accumulate in lysosomes via ion trapping, inducing lysosomal membrane

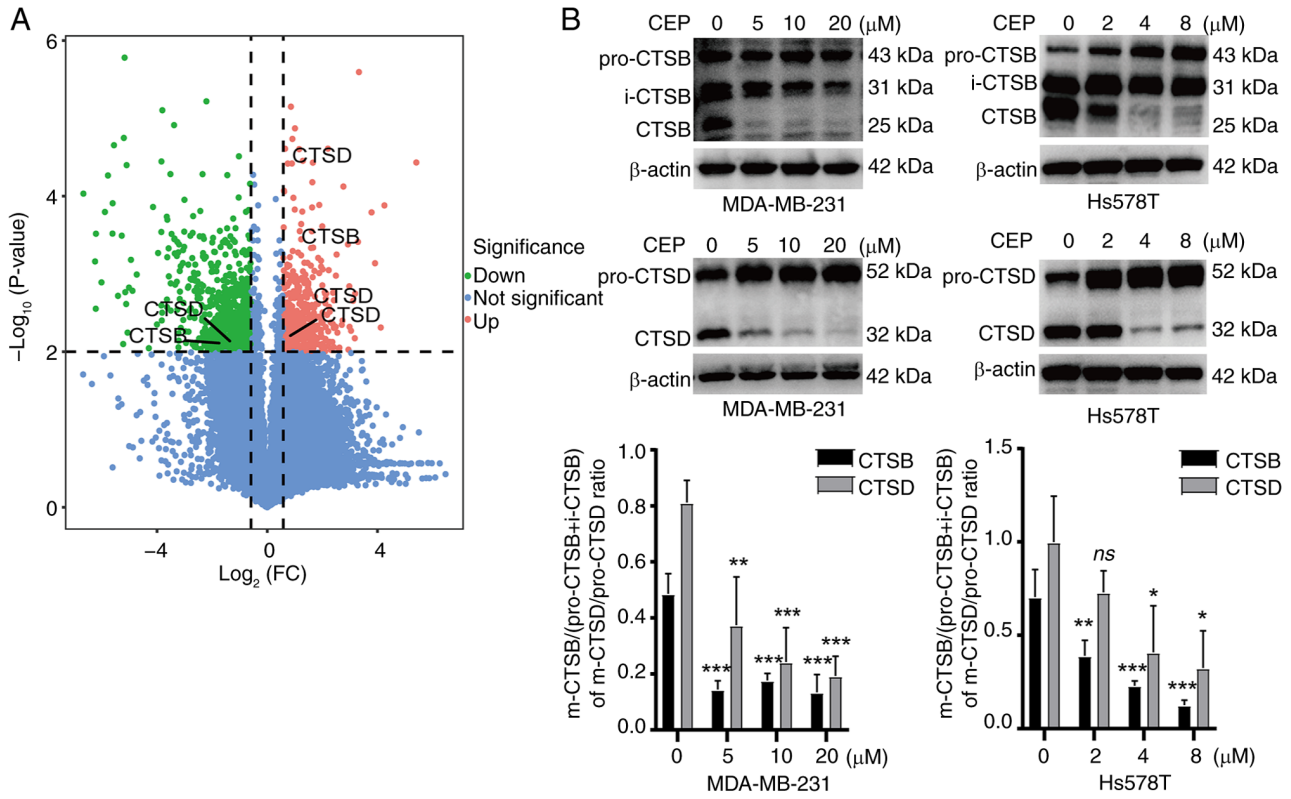

Figure 8. CEP binds to and inhibits lysosomal enzymes. (A) Structurally altered peptides in the MDA-MB-231 cell line upon CEP treatment (10 μM, 1 h; FC >1.5 or <0.667, false discovery rate <1, P<0.01; n=3). (B) CEP treatment suppresses the maturation of CTSB and CTSD (24 h). *P<0.05, **P<0.01 and ***P<0.001 vs. control. CEP, cepharanthine; FC, fold change; CTSD, cathepsin D; CTSB, cathepsin B; pro-CTSB pro-cathepsin B; pro-CTSD, pro-cathepsin D; i-CTSB, inactive cathepsin B; m-CTSB, mature cathepsin B; m-CTSD, mature cathepsin D.

permeabilization (LMP) through detergent-like effects (12-15). These compounds can also disrupt lysosomal function by either neutralizing lysosomal pH or destabilizing membrane-associated enzymes, such as ASAH1, via interactions with anionic lipids (16-20). Due to the presence of a basic isoquinoline group in its structure (21,22), the present study hypothesized that CEP may have induced LMP or disrupted lysosomal function through similar mechanisms. However, the Alexa Fluor 488-dextran retention assay showed no cytoplasmic diffusion after CEP treatment, thereby ruling out induction of LMP in TNBC cells (Fig. 7A). Lysosomal pH was assessed by fluorescence imaging using LysoSensor Green DND-189, a pH-sensitive probe with a fluorescence intensity inversely related to acidity. This assay showed brighter fluorescence of LysoSensor™ Green DND-189 in TNBCs cells, indicating TNBC cells had a reduced lysosomal pH compared with normal breast epithelial cells (Fig. S2), and CEP did not increase the level of lysosomal pH in TNBC cells (Fig. 7B). In addition, CEP caused no significant alterations in the expression of the lysosomal membrane-associated enzymes ASAH1 and SMPD1 (Fig. 7C). The present results suggested that CEP did not promote the degradation of these enzymes in TNBC cells.

To determine whether CEP directly inhibited lysosomal enzymes, the present study performed LiP-MS analysis on TNBC cells. LiP-MS identified 1,163 structurally altered peptides from 663 proteins, including heat shock protein 90α, a known CEP target (Table SII), which confirmed the reliability of the method used in the present study (23). Among these proteins, two lysosomal hydrolases, CTSB, comprising 2 peptides, and CTSD, comprising 4 peptides, exhibited significant conformational changes induced by CEP (Fig. 8A). Western blot analysis further showed that CEP significantly impeded the maturation of CTSB and CTSD, leading to reduced levels of their active forms (Fig. 8B). Taken together, these findings demonstrated that CEP interacted directly with the lysosomal enzymes CTSB and CTSD and hindered their functional activation.

Discussion

Our previous study demonstrated that a low dose of CEP (2 μM) did not induce ΔΨm loss or apoptosis in TNBC cells (24). However, at this concentration, CEP was found to enhance the efficacy of epirubicin against TNBC by blocking autophagic flux, specifically through inhibiting autophagosome-lysosome fusion (24). This finding prompted further investigation into the protein targets and pharmacological mechanisms of CEP in TNBC cells. The present study observed that relatively higher concentrations of CEP could induce ΔΨm loss (10 μM for MDA-MB-231 and 4 μM for Hs578T cells) and promote apoptosis in TNBC cells (10-20 μM for MDA-MB-231 and 2-8 μM for Hs578T cells). This was accompanied by the downregulation of Bcl-2 expression, a result consistent with prior reports in a study performed by Gao *et al* (25). However, in contrast to the study by Gao *et al* (25), the present study did not observe

an upregulation of Bax in TNBC cells. This discrepancy could be attributed to the different time points assessed, as evidenced by the use of 24 h incubations in the present study compared with 48 h incubations in the reported literature. Additionally, the present study showed that CEP upregulated the expression of NOXA, another pro-apoptotic protein in the Bcl-2 family.

Quantitative proteomic analysis revealed significant alterations in the expression of lysosomal proteins following CEP treatment, suggesting the potential inhibition of lysosomal function by CEP. Despite possessing a basic isoquinoline group (21), CEP did not increase lysosomal pH or induce LMP at the concentrations tested in the present study. These observations may have been attributable to the relatively low doses of CEP used, as previous studies indicate that low doses of weakly basic drugs such as chloroquine and clomipramine either fail to elevate or cause only a transient increase in lysosomal pH (26,27). Similarly, induction of LMP by these drugs typically requires higher concentrations, such as 50 μM chloroquine in the 5637 and T24 cell lines and 100 μM chloroquine in HCT116 cells (28,29). The present results of the LiP-MS and western blot analyses provided evidence that CEP bound to the lysosomal hydrolases CTSB and CTSD and inhibited their maturation. These findings demonstrated that CEP suppressed lysosomal degradation through direct enzyme inhibition.

TFEB, a master transcriptional regulator of lysosomal genes, is activated in response to lysosomal damage or inhibition (12). Recent studies have shown that TFEB induces tumor apoptosis by transcriptional upregulation of cyclic AMP-dependent transcription factor ATF-4 (ATF4) and DNA damage-inducible transcript 3 protein (CHOP) expression (30-32). As NOXA and Bcl-2 are transcriptional targets of ATF4 or CHOP (33-35), the present study proposed that CEP may have activated the TFEB/ATF4/CHOP axis, thereby upregulating NOXA and downregulating Bcl-2 expression in TNBC cells. Furthermore, there is evidence that NOXA undergoes degradation via the autophagy-lysosomal pathway, which indicates that autophagy inhibition may prevent NOXA degradation (36-38). Taken together, the findings of the present study and existing literature indicated that CEP induced apoptosis in TNBC cells by regulating NOXA and Bcl-2 expression through lysosomal inhibition of CTSB and CTSD.

Although CEP-mediated lysosomal inhibition remains poorly elucidated, TNBC cells exhibited heightened susceptibility to CEP treatment compared with normal epithelial cells of the MCF10A cell line. This differential sensitivity probably stemmed from the increased dependence of tumor cells on lysosomal function. Studies have shown that tumor cells have a higher proliferation rate and metabolic requirements, which may make them more reliant on lysosome-mediated degradation and recycling pathways (39,40). Consistent with this dependency, tumor cells have been shown to have increased lysosomal abundance and higher lysosomal enzyme expression and activity than normal cells (41-43). As a consequence, lysosomal inhibition would be expected to have more severe effects in malignant cells than in normal cells. Furthermore, tumor cells maintain a lower lysosomal pH than normal cells, a property which is beneficial for the maturation and activity of lysosomal enzymes (44). This acidic environment enhances proton trapping and subsequent accumulation of CEP within the lysosomes. Such preferential accumulation of CEP could have potentially amplified lysosomal inhibition and cytotoxicity toward TNBC cells. The findings of the present study showed that the CEP sensitivity gradient of Hs578T>MDA-MB-231>MCF10A aligned with the gradient of lysosomal acidification across the three cell lines, which supported this possibility.

Due to the methodological constraints of LiP-MS, the present study could not exclude additional CEP-binding lysosomal proteins or non-protein targets. Future investigations are therefore needed to identify CEP interactors within lysosomes. In conclusion, the present study established that CEP directly inhibited lysosomes and triggered mitochondrial apoptosis in TNBC cells, thereby providing a foundation for further investigation of the pharmacological mechanisms of CEP activity.

Acknowledgements

Not applicable.

Funding

The present work was supported by the National Natural Science Foundation of China (grant no. 82004009) and the Science and Technology Plan Program of Guizhou Province (grant no. [2018], 5772-071).

Availability of data and materials

The data generated in the present study are included in the figures and/or tables of this article. The limited proteolysis-coupled mass spectrometry and proteomics data generated in the present study may be found in the iProX database under accession numbers (project ID: IPX0012108000, proteomeXchange ID: PXD064430, password: dFLs; proteomeXchange ID: PXD064550, project ID: IPX0012132000, password: 7eTd) or at the following URLs (https://www.iprox.cn/page/PSV023.html;?url=1748921339238lMbz;https://www.iprox.cn/page/PSV023.html;?url=1748921458718JEnw).

Authors' contributions

LS and DY designed experiments and acquired funding. JL, SZ and YW conducted experiments and collected the data. JL and YW wrote the manuscript. LS and GO analyzed the results and reviewed the manuscript. JL, SZ, YW, GO, DY and LS confirm the authenticity of all the raw data. All authors read and approved the final version of the manuscript.

Ethics approval and consent to participate

Not applicable.

Patient consent for publication

Not applicable.

Competing interests

The authors declare that they have no competing interests.

Use of artificial intelligence tools

During the preparation of this work, Deepseek was used to improve the readability and language of the manuscript, and subsequently, the authors revised and edited the content produced by Deepseek as necessary, taking full responsibility for the ultimate content of the present manuscript.

References

1. Sung H, Ferlay J, Siegel RL, Laversanne M, Soerjomataram I, Jemal A and Bray F: Global cancer statistics 2020: GLOBOCAN estimates of incidence and mortality worldwide for 36 cancers in 185 countries. CA Cancer J Clin 71: 209-249, 2021.
2. Urru SAM, Gallus S, Bosetti C, Moi T, Medda R, Sollai E, Murgia A, Sanges F, Pira G, Manca A, *et al*: Clinical and pathological factors influencing survival in a large cohort of triple-negative breast cancer patients. BMC Cancer 18: 56, 2018.
3. Moss JL, Tatalovich Z, Zhu L, Morgan C and Cronin KA: Triple-negative breast cancer incidence in the United States: Ecological correlations with area-level sociodemographics, healthcare, and health behaviors. Breast Cancer 28: 82-91, 2021.
4. Wu Q, Siddharth S and Sharma D: Triple negative breast cancer: A mountain yet to be scaled despite the triumphs. Cancers (Basel) 13: 3697, 2021.
5. Baranova A, Krasnoselskyi M, Starikov V, Kartashov S, Zhulkevych I, Vlasenko V, Oleshko K, Bilodid O, Sadchikova M and Vinnyk Y: Triple-negative breast cancer: Current treatment strategies and factors of negative prognosis. J Med Life 15: 153-161, 2022.
6. Bianchini G, De Angelis C, Licata L and Gianni L: Treatment landscape of triple-negative breast cancer-expanded options, evolving needs. Nat Rev Clin Oncol 19: 91-113, 2022.
7. Liu K, Hong B, Wang S, Lou F, You Y, Hu R, Shafqat A, Fan H and Tong Y: Pharmacological activity of cepharanthine. Molecules 28: 5019, 2023.
8. Bailly C: Cepharanthine: An update of its mode of action, pharmacological properties and medical applications. Phytomedicine 62, 152956, 2019.
9. Demichev V, Messner CB, Vernardis SI, Lilley KS and Ralser M: DIA-NN: Neural networks and interference correction enable deep proteome coverage in high throughput. Nat Methods 17: 41-44, 2020.
10. Heerdt BG, Houston MA, Wilson AJ and Augenlicht LH: The intrinsic mitochondrial membrane potential (deltapsim) is associated with steady-state mitochondrial activity and the extent to which colonic epithelial cells undergo butyrate-mediated growth arrest and apoptosis. Cancer Res 63: 6311-6319, 2003.
11. Czabotar PE and Garcia-Saez AJ: Mechanisms of BCL-2 family proteins in mitochondrial apoptosis. Nat Rev Mol Cell Biol 24: 732-748, 2023.
12. Lakpa KL, Khan N, Afghah Z, Chen X and Geiger JD: Lysosomal stress response (LSR): Physiological importance and pathological relevance. J Neuroimmune Pharmacol 16: 219-237, 2021.
13. Hu M and Carraway KL III: Repurposing cationic amphiphilic drugs and derivatives to engage lysosomal cell death in cancer treatment. Front Oncol 10: 605361, 2020.
14. Derendorf H: Excessive lysosomal ion-trapping of hydroxychloroquine and azithromycin. Int J Antimicrob Agents 55: 106007, 2020.
15. Zhitomirsky B and Assaraf YG: Lysosomal sequestration of hydrophobic weak base chemotherapeutics triggers lysosomal biogenesis and lysosome-dependent cancer multidrug resistance. Oncotarget 6: 1143-1156, 2015.
16. Fu W, Li X, Lu X, Zhang L, Li R, Zhang N, Liu S, Yang X, Wang Y, Zhao Y, *et al*: A novel acridine derivative, LS-1-10 inhibits autophagic degradation and triggers apoptosis in colon cancer cells. Cell Death Dis 8: e3086, 2017.
17. Ellegaard AM, Bach P and Jäättelä M: Targeting cancer lysosomes with good old cationic amphiphilic drugs. Rev Physiol Biochem Pharmacol 185: 107-152, 2023.
18. Stark M, Silva TFD, Levin G, Machuqueiro M and Assaraf YG: The lysosomotropic activity of hydrophobic weak base drugs is mediated via their intercalation into the lysosomal membrane. Cells 9: 1082, 2020.
19. Gebai A, Gorelik A, Li Z, Illes K and Nagar B: Structural basis for the activation of acid ceramidase. Nat Commun 9: 1621, 2018.
20. Scrima S, Lambrughi M, Favaro L, Maeda K, Jäättelä M and Papaleo E: Acidic sphingomyelinase interactions with lysosomal membranes and cation amphiphilic drugs: A molecular dynamics investigation. Comput Struct Biotechnol J 23: 2516-2533, 2024.
21. Vitello R, Taouba H, Derand M and Liégeois JF: The bis(1,2,3,4-tetrahydroisoquinoline) alkaloids cepharanthine and berbamine are ligands of SK channels. ACS Med Chem Lett 15: 215-220, 2024.
22. Jacob J, Varghese N, Rasheed SP, Agnihotri S, Sharma V and Wakode S: Recent advances in the synthesis of isoquinoline and its analogue: A review. World J Pharm Pharm Sci 5: 1821-1837, 2016.
23. Haginaka J, Kitabatake T, Hirose I, Matsunaga H and Moaddel R: Interaction of cepharanthine with immobilized heat shock protein 90α (Hsp90α) and screening of Hsp90α inhibitors. Anal Biochem 434: 202-206, 2013.
24. Shen LW, Jiang XX, Li ZQ, Li J, Wang M, Jia GF, Ding X, Lei L, Gong QH and Gao N: Cepharanthine sensitizes human triple negative breast cancer cells to chemotherapeutic agent epirubicin via inducing cofilin oxidation-mediated mitochondrial fission and apoptosis. Acta Pharmacol Sin 43: 177-193, 2022.
25. Gao S, Li X, Ding X, Qi W and Yang Q: Cepharanthine induces autophagy, apoptosis and cell cycle arrest in breast cancer cells. Cell Physiol Biochem 41: 1633-1648, 2017.
26. Mlejnek P, Havlasek J, Pastvova N, Dolezel P and Dostalova K: Lysosomal sequestration of weak base drugs, lysosomal biogenesis, and cell cycle alteration. Biomed Pharmacother 153: 113328, 2022.
27. Logan R, Kong AC, Axcell E and Krise JP: Amine-containing molecules and the induction of an expanded lysosomal volume phenotype: A structure-activity relationship study. J Pharm Sci 103: 1572-1580, 2014.
28. Park D and Lee Y: Biphasic activity of chloroquine in human colorectal cancer cells. Dev Rerprod 18: 225-231, 2014.
29. Chen HE, Lin JF, Lin YC, Wen SI, Yang SC, Tsai TF, Chou KY and Hwang IST: Chloroquine induces lysosomal membrane permeability-mediated cell death in bladder cancer cells. Formos J Surg 51: 133-141, 2018.
30. Franco-Juárez B, Coronel-Cruz C, Hernández-Ochoa B, Gómez-Manzo S, Cárdenas-Rodríguez N, Arreguin-Espinosa R, Bandala C, Canseco-Ávila LM and Ortega-Cuellar D: TFEB; beyond its role as an autophagy and lysosomes regulator. Cells 11: 3153, 2022.
31. Yang CB, Liu J, Tong BC, Wang ZY, Zhu Z, Su CF, Sreenivasmurthy SG, Wu JX, Iyaswamy A, Krishnamoorthi S, *et al*: TFEB, a master regulator of autophagy and biogenesis, unexpectedly promotes apoptosis in response to the cyclopentenone prostaglandin 15d-PGJ2. Acta Pharmacol Sin 43: 1251-1263, 2022.
32. Martina JA, Diab HI, Brady OA and Puertollano R: TFEB and TFE3 are novel components of the integrated stress response. EMBO J 35: 479-495, 2016.
33. Zhao X, Kong F, Wang L and Zhang H: c-FLIP and the NOXA/Mcl-1 axis participate in the synergistic effect of pemetrexed plus cisplatin in human choroidal melanoma cells. PLoS One 1: e0184135, 2017.
34. Núñez-Vázquez S, Sánchez-Vera I, Saura-Esteller J, Cosialls AM, Noisier AFM, Albericio F, Lavilla R, Pons G, Iglesias-Serret D and Gil J: NOXA upregulation by the prohibitin-binding compound fluorizoline is transcriptionally regulated by integrated stress response-induced ATF3 and ATF4. FEBS J 288: 1271-1285, 2021.
35. Armstrong JL, Flockhart R, Veal GJ, Lovat PE and Redfern CP: Regulation of endoplasmic reticulum stress-induced cell death by ATF4 in neuroectodermal tumor cells. J Biol Chem 285: 6091-6100, 2010.
36. Kuroda Y, Koyama D, Kikuchi J, Mori S, Ichinohe T and Furukawa Y: Autophagic degradation of NOXA underlies stromal cell-mediated resistance to proteasome inhibitors in mantle cell lymphoma. Leuk Res 111: 106672, 2021.
37. Wang J, Cui D, Gu S, Chen X, Bi Y, Xiong X and Zhao Y: Autophagy regulates apoptosis by targeting NOXA for degradation. Biochim Biophys Acta Mol Cell Res 1865: 1105-1113, 2018.

38. Moriya S, Kazama H, Hino H, Takano N, Hiramoto M, Aizawa S and Miyazawa K: Clarithromycin overcomes stromal cell-mediated drug resistance against proteasome inhibitors in myeloma cells via autophagy flux blockage leading to high NOXA expression. PLoS One 18: e0295273, 2023.
39. Davidson SM and Vander Heiden MG: Critical functions of the lysosome in cancer biology. Annu Rev Pharmacol Toxicol 57: 481-507, 2017.
40. Zhang Z, Yue P, Lu T, Wang Y, Wei Y and Wei X: Role of lysosomes in physiological activities, diseases, and therapy. J Hematol Oncol 14: 79. 2021.
41. Chen R, Jäättelä M and Liu B: Lysosome as a central hub for rewiring pH homeostasis in tumors. Cancers (Basel) 12: 2437, 2020.
42. Serrano-Puebla A and Boya P: Lysosomal membrane permeabilization as a cell death mechanism in cancer cells. Biochem Soc Trans 46: 207-215, 2018.
43. Kirkegaard T and Jäättelä M: Lysosomal involvement in cell death and cancer. Biochim Biophys Acta 1793: 746-754, 2009.
44. Kroemer G and Jäättelä M: Lysosomes and autophagy in cell death control. Nat Rev Cancer 5: 886-897, 2005.